Electronic Supplementary Material for: Is there a brainstem substrate for action selection?

Electronic Supplementary Material A provides a summary of the stochastic anatomical model that constructs a network with the proposed cluster structure of the mRF.

Electronic Supplementary Material B both gives the parameter values used to assess the wiring efficiency of the cluster structure, and looks at the results in more detail.

Electronic Supplementary Material C gives the full mathematical description of the population-level mRF model, and the parameter values used for the example simulations described in the main text.

Electronic Supplementary Material D looks at the detailed results from the assessment of the robustness of selection in the sub-action configuration of the mRF.

A Anatomical models of the mRF

As briefly described in the main text, we specified a *stochastic* model that generated a network with the proposed cluster organisation of the mRF. Every one of the N_c clusters in the network has n neurons (the total number of neurons — nodes — within the model is thus $T = N_c \times n$). Within each cluster a certain proportion ρ of neurons are deemed to be the projection neurons, the remainder are inter-neurons. From the data reviewed in Humphries et al. (2006), we set bounds $0.7 \leq \rho < 0.9$.

Three parameters define the connections — links – between neurons. For each projection neuron, the probability of forming a connection c between itself and another cluster is $P(c)$. The probability of each projection neuron contacting a given cluster is $P(c)$. This models the probability of the projection neuron's axon extending a collateral into that cluster. Two model variants were defined by two choices of distribution for $P(c)$. Data from Grantyn et al. (1987) suggests a spatially uniform distribution of axon collaterals, with a probability of $P(c) = 0.25$ for all clusters. In contrast, McCulloch and colleague's RF model (Kilmer et al., 1969) used a distance-dependent distribution of collaterals (William Kilmer, personal communication), typical of models of neural connectivity (Hellwig, 2000). Thus, if there are d intervening clusters between the projection neuron and the target cluster then $P(c) = d^{-a}$ (for adjacent clusters $d = 1$); we use $a = 1$ throughout.

If a collateral is extended, then $P(p)$ is the probability of the projection neuron forming a connection with any given neuron in that cluster. Finally, $P(l)$ denotes the probability of an inter-neuron making a connection with any other given neuron in its own cluster. Mathematically, when we construct a particular instantiation of the stochastic anatomical model, the above parameters are used to define directed edges (links) in a connectivity graph G, where each vertex (node) of the graph is labeled as being either a projection or an inter-neuron.

We proposed a further model in which the connections were defined by a procedure analogous to the neural development process, rather than a stochastic model of the final, adult configuration of the neural structure. We begin with a structure representing the overgrown synaptic density with all cells in position, using the just-described stochastic model with connection probabilities

set to high values ($P(l) = P(p) = 0.9$). We then repeat a process of synaptic weight change (representing plasticity due to learning and sensory experience) and synaptic pruning (deletion of weak synapses) that may occur in the RF during the post-natal period. The process terminates when a target total number of synapses is reached (a target number of synapses based on specified target probabilities of projection neuron connections t_p and inter-neuron connections t_l). We refer to this as the *pruning* model: for further details and parameterisation see Humphries et al. (2006).

B Wiring efficiency of the cluster structure

The total axonal wire length for a cluster model was computed as follows. A simple geometrical model of the mRF was constructed in which each of the n nodes was assigned a randomly determined three-dimensional position within its parent cluster, limited by the cluster dimensions of 2 mm wide $\times$ 2 mm high $\times$ 0.2 mm deep (width and height of the mRF estimated from the UCLA Laboratory Of Neural Imaging (LONI) rat brain atlases, www.loni.ucla.edu).

To create the cluster model networks, we fixed values of $N_c = 35, n = 50$ and $\rho = 0.8$. Both stochastic and pruning models (parameter values from Humphries et al., 2006) were assessed, varying $P(p)$ (resp. t_p) and $P(l)$ (resp. t_l) over the interval [0.1,0.5] in steps of 0.1, and repeating for each of the spatially-uniformly and distance-dependent collateral distributions. For each of the 25 instantiations of each anatomical-model and collateral-distribution combination we created two sets of comparable random networks — a randomly-wired set and a randomly-positioned set – as described in the main text.

By comparing the total wire-lengths of the cluster model network and random networks, we were testing two hypotheses of wiring efficiency: (H1) the cluster structure could reduce the wiring connecting together neurons fixed in particular positions: that is, the neuron placement is critical, for example due to the position of input fibres, and the wiring is arbitrary to some extent; (H2) the cluster structure could reduce the length of wiring required to achieve a particular network configuration: that is, the internal wiring is critical and the neuron position is arbitrary to some extent.

The detailed results are shown in Figure S1. The total wiring length for the randomly-wired network was always lower than for the comparable cluster model network: we thus reject H1. By contrast, the total wiring length for the randomly-positioned network was always higher than for the comparable cluster model network: we thus have evidence for H2.

Our rejection of H1 is contrary to the results of Mathias and Gopal (2001). They demonstrated that, in a one-dimensional ring lattice with regularly spaced nodes, small-world networks were formed when attempting to the find the optimal trade-off between total wire length and shortest path length. Our results suggest their findings do not carry over to graphs in which the nodes are irregularly spaced or placed in three dimensions, but further work is required for a rigorous demonstration. Nevertheless, the evidence for H2 suggests small-world networks may help optimise component placement for the three-dimensional instantiation of a given graph.

C Population-based model of the mRF

We detail here the extensions to the stochastic anatomical model necessary to incorporate afferent inputs to the mRF, followed by the mathematical description of the population-level model of the mRF.

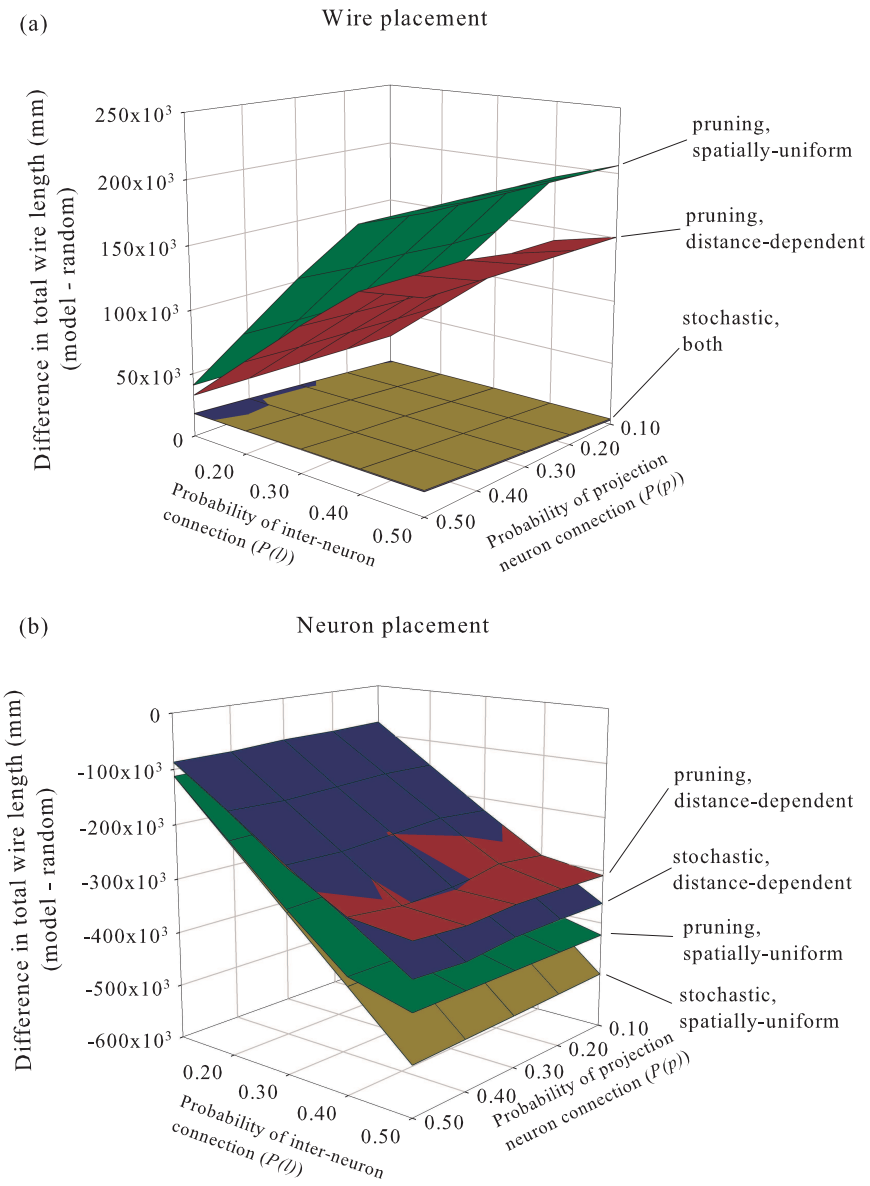

Figure S1: Wiring optimisation of the cluster structure. The horizontal plane axes give the values of the connection probabilities tested. The vertical axes give the resulting difference in total wiring lengths between the cluster model network and the corresponding random network. (a) Randomly-wired networks: For given set of node positions, randomly wiring the same number of connections always results in a lower total wire length than the cluster structure. We thus reject H1. (b) Randomly-positioned networks: For a given set of connected nodes, randomly positioning the nodes always results in a greater total wire length than the cluster structure. There is thus evidence for H2.

C.1 Incorporating afferent input

Two parameters are added to the anatomical models to define the proportion of neurons that receive afferent input: a proportion of projection neurons ρ_s and a proportion of interneurons λ_s are defined as receiving afferents within each cluster. Given the extent and morphology of their dendritic trees, it is likely that the projection neurons within a cluster will receive synaptic input from the majority of afferents contacting that cluster. In addition, projection neurons which do not respond to some form of sensory or physiological stimulation are rare (Schulz et al., 1983). Thus we set $\rho_s = 1$ throughout.

Patterning of external inputs to the inter-neurons is unknown, but a similar argument, based on dendritic morphology, suggests proportionally fewer inter-neurons than projection neurons would receive input from the same afferent to their cluster. Some medium-sized RF neurons, potentially inter-neurons, do receive spinal input (Eccles et al., 1976), and thus information-carrying input to inter-neurons cannot be entirely ruled out. We would thus allow λ_s to vary over the interval $[0, 0.5]$ in a full exploration of the model.

C.2 Mathematical description

Following the anatomical model (Humphries et al., 2006), we assume that all projection neurons are excitatory and all inter-neurons inhibitory. For cluster k, its normalised, mean projection neuron firing rate c_k is given by

$$\tau \frac{dc_k(t)}{dt} = -c_k(t) + F\Big(\bar{w}_e \sum_{j=1}^{N_c} A_{jk}\, c_j(t) + \bar{w}_i b_k i_k(t) + \rho_s u_k(t)\Big), \tag{1}$$

where τ is a time constant dictating the decay rate of the neural activity, $F(x)$ is the neural output function, $\bar{w}_e, \bar{w}_i$, are the mean excitatory and inhibitory weights, $c_j(t)$ is the average projection neuron output from cluster j, and $u_k(t)$ is input to the current cluster.

The normalised mean inter-neuron firing rate i_k of cluster k is given by

$$\tau \frac{di_k(t)}{dt} = -i_k(t) + F\left(\bar{w}_e \sum_{j=1}^{N_c} C_{jk}\, c_j(t) + \bar{w}_i d_k\Big(i_k(t) - \frac{i_k(t)}{n^-}\Big) + \lambda_s u_k(t)\right), \tag{2}$$

where $n^- = n(1-\rho)$ is the number of inter-neurons per cluster — the bracketed term containing this parameter describes the contribution of the inter-neuron population to itself. Variables A_{jk}, b_k, C_{jk}, d_k are scalars determined from the properties of the underlying anatomical model (section A): A_{jk}, C_{jk} are the mean number of contacts from afferent cluster j to, respectively, the projection and inter-neurons of cluster k; b_k, d_k are the mean number of contacts from inter-neurons in the current cluster k to, respectively, the projection and inter-neurons in that same cluster.

We use a single input variable u_k, interpreted as the normalised scalar summation of all afferent input to cluster k, and which thus represents the salience of that cluster's represented action. The majority of sensory inputs are assumed to be excitatory, as firing rate increases are generally reported following the presentation of stimuli. However, inhibitory responses have been reported following both visceral and somatic stimulation (Langhorst et al., 1996), which may reflect either direct inhibitory input, or indirect inhibition via afferent drive of the inhibitory inter-neurons. Thus, we are not able to state definitively that sensory input is entirely excitatory, and must therefore consider u_k over the interval [-1,1] in a full exploration of the model — to

simplify the simulations in the main text, we considered u_k only over the interval [0,1], as excitatory inputs are most consistently reported.

The output function is a piece-wise linear approximation to a sigmoidal function given by

$$F(x) = \begin{cases} 0, & \text{if } x < \epsilon; \\ m(x-\epsilon), & \text{if } \epsilon \leq x \leq 1/m + \epsilon \\ 1, & \text{if } x > 1/m + \epsilon \end{cases} \tag{3}$$

where m is slope, and ϵ the threshold of the output function. Throughout, we set $m = 1$ and $\epsilon = 0$.

C.3 Computational model parameter values

The example simulations reported in the main text to illustrate the configurations of the mRF were based on a single instantiation of the anatomical model. A stochastic anatomical model network containing just $N_c = 3$ clusters, each with $n = 100$ neurons, was constructed, with the parameter set: $P(l) = P(p) = 0.1$, as arbitrarily chosen neuron pairs are likely to have low connection probabilities (Schuz, 1995); $\rho = 0.8$, as this is the middle of the range of projection neuron proportions; and $\lambda_s = 0$, so that we need only consider effects of sensory inputs to the projection neurons — however, increasing λ_s to its maximum value ($\lambda_s = 0.5$) did not alter the relative values of the output reported in the main text.

For the population-level model, we used the following parameter values. The population activity time constant $\tau = 0.005$s, to reflect the short membrane time constant of the large-bodied neurons (Yen and Chan, 1993; Serafin et al., 1996). Each example simulation has the same continuous (i.e. $\mathbf{u}(t) = \mathbf{u}$) input pattern, $\mathbf{u} = [0.4\ 0.3\ 0.2]$. The ODE system described by equations (1) and (2) was solved numerically using the variable-step Runge-Kutta solver in MatLab (MathWorks), with initial conditions $c_k(0) = i_k(0) = 0$, and the cluster outputs were recorded after equilibrium was reached.

We set $\bar{w}_e = 0.2$ because the influence of a single excitatory neuron on a target neuron is far less than a one-to-one mapping of firing rates (which would be implied by $w_e = 1$). The value for w_i was then derived. The work of Jones et al. (1991) suggests the relative proportions of inhibitory and excitatory synapses on projection neurons are approximately equal. Yet, there are far fewer inhibitory sources in the mRF than there are excitatory sources. Thus, we believe there is a case for adopting the strict relation $\bar{w}_e < \bar{w}_i$ in the population-level model. A simple approximation to the percentage synapse distribution is to determine the total number of excitatory N_e and inhibitory N_i connections in an anatomical model and set $\bar{w}_i = -\bar{w}_e \times N_e/N_i$, thereby setting the total absolute weight for excitatory and inhibitory units to be equal (and thereby approximating the synaptic distribution on the projection neurons). For the example simulations described here, $\bar{w}_i = -0.2 \times 1176/573 = -0.41$.

The particular mRF anatomical model network created for the simulations gave connection parameter matrices for the computational model of:

$$\mathbf{A} = \begin{bmatrix} 0 & 1.61 & 1.57 \\ 2.15 & 0 & 2.09 \\ 2.03 & 2.49 & 0 \end{bmatrix} \qquad \mathbf{b} = \begin{bmatrix} 1.7 \\ 2.14 \\ 2.03 \end{bmatrix}$$

$$\mathbf{C} = \begin{bmatrix} 0 & 1.5 & 1.5 \\ 1.7 & 0 & 2.5 \\ 1.85 & 2.05 & 0 \end{bmatrix} \qquad \mathbf{d} = \begin{bmatrix} 1.8 \\ 1.55 \\ 2.1 \end{bmatrix}.$$

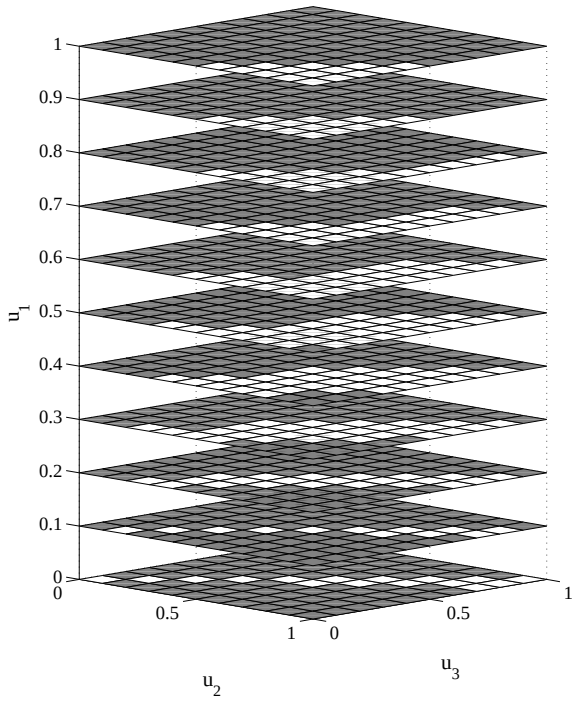

Figure S2: Output states of the sub-action configuration. Correct selections (grey squares) occurred following the majority of inputs. Incorrect selections (white squares) occurred around the input values for which u_2 was roughly equal to either or both of u_1 and u_3 — where only one of these was roughly equal, the other of that pair was closer to zero.

For the sub-action configuration discussed in the main text (section 4.c.ii), **A** and **C** are altered to match the connection pattern shown in Figure 4c (of the main text), thus

$$\mathbf{A} = \begin{bmatrix} 0 & 0 & 1.57 \\ 2.15 & 0 & 0 \\ 2.03 & 0 & 0 \end{bmatrix} \quad \mathbf{C} = \begin{bmatrix} 0 & 1.5 & 0 \\ 1.7 & 0 & 2.5 \\ 0 & 2.05 & 0 \end{bmatrix}.$$

D Robustness of sub-action selection

The full results of the batch of simulations detailed in the main text are shown in Figure S2.

References

Eccles, J. C., Nicoll, R. A., Rantucci, T., Taborikova, H., and Willey, T. J. (1976). Topographic studies on medial reticular nucleus. *J. Neurophysiol.*, 39:109–118.

Grantyn, A., Ong-Meang Jacques, V., and Berthoz, A. (1987). Reticulo-spinal neurons participating in the control of synergic eye and head movements during orienting in the cat. II. Morphological properties as revealed by intra-axonal injections of horseradish peroxidase. *Exp. Brain Res.*, 66:355–377.

Hellwig, B. (2000). A quantitative analysis of the local connectivity between pyramidal neurons in layers 2/3 of the rat visual cortex. *Biol. Cybern.*, 82:111–121.

Humphries, M. D., Gurney, K., and Prescott, T. J. (2006). The brainstem reticular formation is a small-world, not scale-free, network. *Proc. Roy. Soc. B.*, 273:503–511. doi:10.1098/rspb.2005.3354.

Jones, B. E., Holmes, C. J., Rodriguez-Veiga, E., and Mainville, L. (1991). GABA-synthesizing neurons in the medulla: their relationship to serotonin-containing and spinally projecting neurons in the rat. *J. Comp. Neurol.*, 313:349–367.

Kilmer, W. L., McCulloch, W. S., and Blum, J. (1969). A model of the vertebrate central command system. *Int. J. Man Mach. Stud.*, 1:279–309.

Langhorst, P., Schulz, B. G., Seller, H., and Koepchen, H. P. (1996). Convergence of visceral and somatic afferents on single neurones in the reticular formation of the lower brain stem in dogs. *J. Auton. Nerv. Syst.*, 57:149–157.

Mathias, N. and Gopal, V. (2001). Small worlds: How and why. *Phys. Rev. E*, 63:021117.

Schulz, B., Lambertz, M., Schulz, G., and Langhorst, P. (1983). Reticular formation of the lower brainstem. A common system for cardiorespiratory and somatomotor functions: discharge patterns of neighboring neurons influenced by somatosensory afferents. *J. Auton. Nerv. Syst.*, 9:433–449.

Schuz, A. (1995). Neuroanatomy in a computational perspective. In Arbib, M. A., editor, *The Handbook of Brain Theory and Neural Networks*, pages 622–626. MIT Press, Cambridge, MA.

Serafin, M., Vidal, P. P., and Muhlethaler, M. (1996). Electrophysiological study of nucleus gigantocellularis neurons in guinea-pig brainstem slices. *Neuroscience*, 73:797–805.

Yen, J. C. and Chan, S. H. (1993). Passive biophysical membrane properties of nucleus reticularis gigantocellularis neurons in brain slices from the rat. *Neurosci. Lett.*, 159:5–8.